Accurately Disentangling Core and Winding Losses in Experimental, *In-situ* Magnetic Loss Measurement for Power Electronic Circuits and Applications

Lifang Yi, *Student Member*, *IEEE*, Jinyeong Moon, *Senior Member*, *IEEE*

***Abstract*—This paper presents a new idea that enables direct, high-precision, *in-situ*, and in-operation core loss measurement in experiment. Coupled with the improved dual-curve derivative (iDCD) method that provides accurate *in-situ* total magnetic loss measurement, this paper can accurately and experimentally disentangle the core and winding losses from the lumped magnetic loss *in-situ* and in-operation for practical power electronic converters. Historically, the timing skew between measurement channels has plagued direct power loss measurement approaches, especially for switched-mode power electronics whose voltage and current waveforms are both AC (e.g., excited by rectangular and triangular stimuli). This unknown timing skew severely hinders the application of the conventional "two-winding method" for magnetic core loss measurement, introducing challenges when attempting to measure the power loss under desired operating conditions. This paper builds a comprehensive mathematical model to analyze the effect of the timing skew on the direct core loss measurement and presents a novel approach based on a capacitor branch to eliminate the measurement error caused by the unknown timing skew. The proposed method provides an extremely tight error tolerance at a sub-1% level. A new cross-validation method - though is only suitable in highly controlled lab settings and is less accurate - is developed to demonstrate the proposed method's efficacy and prove that the proposed method can be freely applied beyond lab settings. Theoretical analysis is verified in simulation and experiment with a conventional DC-DC step-down buck converter with non-sinusoidal voltage and current waveforms under a range of practical circuit parameters.**

***Index Terms*—Direct, *in-situ*, Magnetic, Inductor, Core, Power, Loss, Measurement, Timing, Skew, DC-DC, Converter**

I. Introduction

The continuous advancements in power semiconductor devices, topologies, and control methodologies have revolutionized the efficiency and power density of power electronic circuits [1]–[3]. As a consequence, the proportion of magnetic loss in the overall losses of the converter has gained significance, highlighting the importance of reducing magnetic losses [4]. The optimization of magnetics has emerged as a critical factor in improving the efficiency and reducing the size and weight of power converters. To validate the optimization and design of the magnetics, it is essential to measure the magnetic component's loss while it is operating under the intended conditions. This ensures that the magnetics are performing as expected and meeting the desired performance criteria in their rightful place.

Measuring the loss of a magnetic component when it is operating in the converter is a challenging task. This challenge arises primarily due to the inherent and unpredictable timing skew between measurement channels, given that both its voltage and current operate in an AC (alternating current) mode. Consequently, in a real test, the magnetic loss is often estimated relying on a deduction method, where all losses except the magnetic one in the converter are excluded from consideration [5], [6]. However, this deduction method can only provide a relatively broad and imprecise estimation due to the lack of a thorough understanding of other components' loss mechanisms, such as the losses in FETs. Thus, it falls short in offering the adequate level of precision required for design verification of modern power electronics. In some cases, the performance of the entire converter is used as an indirect indicator of whether the magnetic component's design meets the requirements. If the converter's loss exceeds expectations, the magnetic component's design is often blamed. Such an approach is irrational and lacks rigor for design verification.

Power loss measurement through a calorimeter is a conventional approach [7]–[9]. The temperature rise of the coolant, along with a suitable thermal resistance model, can be used to estimate the total power loss of a magnetic component. However, this method is indirect and relies on the accuracy of the 3rd party data, such as the heat capacity, thermal resistance, and thermal capacitance of the medium. The accuracy of these data points can vary and may introduce uncertainties in the power loss measurement. This method cannot be considered strictly *in-situ* as it introduces changes to the electrical properties of the magnetic component when it is placed in a different dielectric medium. The alteration in the dielectric medium can impact the overall behavior and characteristics [10], [11], such as inter-winding capacitances, natural resonant frequency, and dielectric loss. In addition, the calorimetric method necessitates specialized equipment and expertise, making it time-consuming in practical applications. This approach also has limitations regarding the range of power loss it can accurately measure, unsuitable for cases where the power loss is either excessively small or large. Furthermore, the loss measured with a calorimeter represents the total power loss of the magnetic component, including both the core loss and winding loss. Disentangling the core and winding losses from the total power loss remains a formidable challenge. This separation is particularly crucial for verifying the magnetic design, especially when the design concentrates on optimizing either the core or the winding separately.

To estimate the core loss alone, the Steinmetz equation [12] or one of its numerous variations [13] [14] are frequently employed. Three key Steinmetz parameters (k, α, and β) are typically provided by manufacturers for loss prediction of magnetic core material within a specific operating range. The

original Steinmetz equation is limited to sinusoidal excitation within a narrow operating range and does not adequately handle DC bias or multiple/local magnetic hysteresis loops. There have been efforts to enhance the applicability and accuracy of the original Steinmetz in expanded settings – notably modified Steinmetz Equation (MSE) [15], Generalized Steinmetz Equation (GSE) [16], improved Generalized Steinmetz Equation (iGSE) [17], etc. However, the accuracy of the calculated magnetic core loss is still limited to a narrow range. Instead of relying on a 3rd party data and various fitting equations, a more preferable approach for accurate magnetic characterization would be to develop a customized loss map that covers all the intended operating conditions and incorporates all the necessary considerations. To create such a loss map *in-house*, it is essential to measure the power loss of a magnetic component *in-situ* while the converter is in operation. Furthermore, the necessity of *in-situ* power loss measurement still arises even if we trust a magnetics design based on Steinmetz parameters because the design still needs to be validated through experiments.

The two-winding method is commonly used to directly measure magnetic core loss and is theoretically valid for arbitrary excitation [18]. However, the measured loss of this method is sensitive to the timing skew between measurement channels, especially for high-frequency applications. The capacitive cancellation method presented in [19] and the inductive cancellation method discussed in [20] can reduce its sensitivity to the timing skew. However, they are both vulnerable to additional measurement errors and face challenges associated with the selection of appropriate components. The enhanced partial cancellation method, introduced in [21], eliminates the need for fine-tuning the values of cancellation components. However, the accuracy of the partial cancellation method relies on the effectiveness of the cancellation process [22]. This method only corrects the timing skew caused by the difference in the probes and the measurement loops leading to the oscilloscope. Other error sources, such as the delay caused by circuit components and printed circuit board (PCB) layout, are not considered, which are the main culprits in precision measurements. In addition, these methods tend to be more complex as they involve the utilization of additional components that are relatively large, which will likely change the overall operation of the circuit. Consequently, the waveforms obtained during the measurement may exhibit significant deviations from the intended target operational behavior of interest.

The unknown timing skew between measurement channels becomes the biggest practical challenge preventing this simple two-winding method in reality [23]. In power electronic circuits, magnetic components often operate under rectangular – non-sinusoidal – voltage excitation. In our previous work [5], [6], [24], [25], we have dedicated our efforts to achieving precise *in-situ* measurement of inductor loss (i.e., the sum of the core and winding losses) under rectangular voltage excitation, effectively eliminating any errors introduced by timing skew. This paper aims to directly measure the core loss *in-situ* instead of the total inductor loss. The mathematical model will be built to analyze the effect of the timing skew on the measured core loss. Rather than attempting to reduce the measurement sensitivity to timing skew, a more effective approach is proposed in this paper to accurately determine the unknown timing skew and directly eliminate the error related to the timing skew. A small additional capacitor at a single-digit or low two-digit pF level will be utilized to introduce a special geometric feature to the mathematical model, which will facilitate the identification of the actual timing skew and the core loss. Through simulation and experimental validation, the proposed method will be proven effective, accurate, and practical for direct *in-situ* measurement of the magnetic core loss under rectangular voltage excitation. When coupled with the total magnetic loss measured using the iDCD method introduced in [25], the proposed core loss measurement method offers separation of core and winding losses in experiment, *in-situ*, and in-operation with unprecedented precision. Our method can finally close the design and optimization loop of magnetic components and power electronic converters and transparently translate the design effort into visible performance gains in magnetics and power converters.

II. Mathematical Model between Core Loss and Timing Skew

Here, an inductor operating in a DC-DC step-down buck converter is considered as an example to build the mathematical model. The main variables of the circuit are: V_H [V] - input voltage; V_L [V] - output voltage; f [Hz] - switching frequency; L [H] - inductance; S [V/s] - slope of voltage transitions; and θ [s] - timing skew. The steady-state waveforms of voltage and current of an ideal inductor, $V_{\rm ind}$ and $I_{\rm ind}$, are shown in the upper and lower plots of Fig. 1, respectively. The current waveform, illustrated in thick red, indicates that the measured current lags the voltage by θ. According to the guidelines without and with timing skew, waveforms in one switching cycle can be divided into eight regions as shown in Fig. 1.

Considering the loss mechanisms of a real inductor, a lossy inductor model is shown in Fig. 2, including an ideal inductor (L), a resistor in parallel (R_p) to lump core loss, and a resistor in series (R_s) to lump winding loss [24]. The equivalent circuit of the inductor under two-winding test is also provided in Fig. 2. To directly measure the core loss, the voltage across the magnetic core ($V_{\rm ind}$) and the current through the inductor ($I_{\rm ind,all}$) should be obtained when the inductor is operating in the converter under the desired conditions. An auxiliary winding is employed to extract the core voltage, $V_{\rm core}$, on the secondary side. The turns ratio is set to unity to simplify the analysis.

$$\begin{cases} I_{\rm ind,all}\left(t\right) = \ I_{\rm ind}\left(t\right) + \dfrac{V_{\rm ind}\left(t\right)}{R_p} \\ V_{\rm core}\left(t\right) = \ V_{\rm ind}\left(t\right) \end{cases} \tag{1}$$

Although R_s and R_p are frequency-dependent and nonlinear resistors in reality, it can be shown that they do not affect the mathematical model and the method developed in this article. The key requirement is that the behavior of R_s and R_p remains consistent and repeatable in switching cycles (i.e., as long as the magnetic component stably establishes the steady-state).

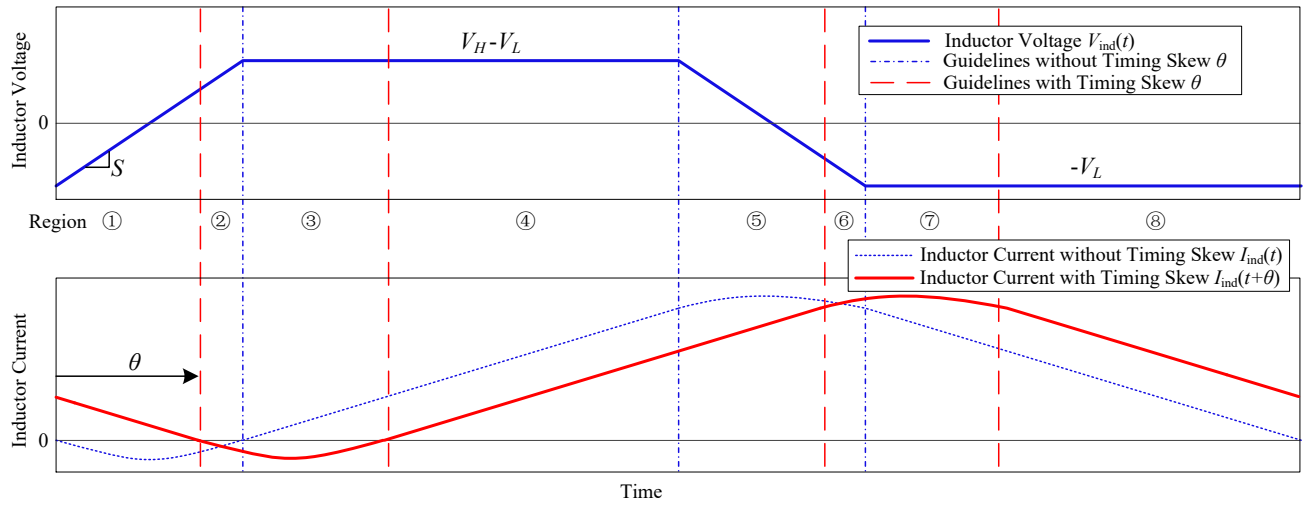

Fig. 1. Inductor voltage and current waveforms with a positive timing skew ($0 \le \theta \le \frac{V_H}{S}$) - current lagging

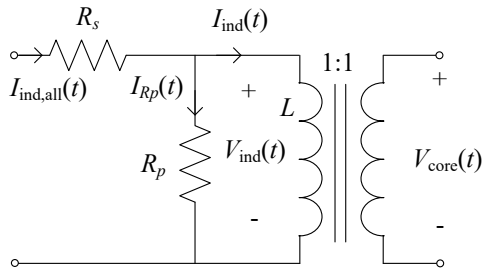

Fig. 2. Equivalent circuit model of the inductor for two-winding test

Without timing skew (i.e., $\theta = 0$), the measured core loss, $P_{\text{Core}}^{\text{Meas}}(\theta)$, must be identical to the real core loss, $P_{\text{Core}}^{\text{Real}}$.

$$P_{\text{Core}}^{\text{Meas}}(\theta)\,|_{\theta=0} = P_{\text{Core}}^{\text{Real}}. \tag{2}$$

Assuming the measured current lags the voltage by θ, the sensitivity of the measured core loss with respect to the timing skew, $\partial P_{\text{Core}}^{\text{Meas}}(\theta)/\partial\theta$, can be calculated as

$$\frac{\partial P_{\text{Core}}^{\text{Meas}}(\theta)}{\partial\theta} = \frac{\partial}{\partial\theta}\left[\frac{1}{T}\int_{t_0}^{t_0+T} V_{\text{ind}}(t)\left(I_{\text{ind}}(t+\theta)+\frac{V_{\text{ind}}(t+\theta)}{R_p}\right)\mathrm{d}t\right]. \tag{3}$$

Here assumed is that the current lags the voltage by θ, where $0 \le \theta \le \frac{V_H}{S}$. When the current leads the voltage (i.e., $-\frac{V_H}{S} \le \theta \le 0$), the mathematical derivation can be similarly done. The expressions of $V_{\text{ind}}(t)$, $I_{\text{ind}}(t+\theta)$ and $V_{\text{ind}}(t+\theta)$ under a rectangular voltage excitation in eight regions are provided in the previous work [6], [24]. Combining the integration results in eight regions, when $-\frac{V_H}{S} \le \theta \le \frac{V_H}{S}$, the sensitivity of the measured core loss with respect to the timing skew can be calculated as

TABLE I
MAIN CIRCUIT PARAMETERS

V_H	V_L	f	S
30 V	15 V	100 kHz	5 V/ns
L	R_p	R_s	$C_{p,\text{add}}$
10 µH	5 kΩ	0.2 Ω	12 pF

$$\frac{\partial P_{\text{Core}}^{\text{Meas}}(\theta)}{\partial\theta} = \begin{cases} * -\frac{S^2 f}{3L}\theta^3 + \left(\frac{V_H S f}{L} + \frac{S^2 f}{R_p}\right)\theta^2 - \frac{2V_H f S}{R_p}\theta \\ \quad -\left(\frac{V_L(V_H - V_L)}{L} - \frac{V_H^3 f}{3LS}\right) \\ \dagger \quad \frac{S^2 f}{3L}\theta^3 + \left(\frac{V_H S f}{L} - \frac{S^2 f}{R_p}\right)\theta^2 - \frac{2V_H f S}{R_p}\theta \\ \quad -\left(\frac{V_L(V_H - V_L)}{L} - \frac{V_H^3 f}{3LS}\right) \\ *\left[\text{For } 0 \le \theta \le \frac{V_H}{S}\right], \dagger\left[\text{For } -\frac{V_H}{S} \le \theta \le 0\right]. \end{cases} \tag{4}$$

According to (2) and (4) , the measured core loss with respect to the timing skew can be expressed as

$$P_{\text{Core}}^{\text{Meas}}(\theta) = \begin{cases} * -\frac{S^2 f}{12L}\theta^4 + \left(\frac{V_H S f}{3L} + \frac{S^2 f}{3R_p}\right)\theta^3 - \frac{V_H f S}{R_p}\theta^2 \\ \quad -\left(\frac{V_L(V_H - V_L)}{L} - \frac{V_H^3 f}{3LS}\right)\theta + P_{\text{Core}}^{\text{Real}} \\ \dagger \quad \frac{S^2 f}{12L}\theta^4 + \left(\frac{V_H S f}{3L} - \frac{S^2 f}{3R_p}\right)\theta^3 - \frac{V_H f S}{R_p}\theta^2 \\ \quad -\left(\frac{V_L(V_H - V_L)}{L} - \frac{V_H^3 f}{3LS}\right)\theta + P_{\text{Core}}^{\text{Real}} \\ *\left[\text{For } 0 \le \theta \le \frac{V_H}{S}\right], \dagger\left[\text{For } -\frac{V_H}{S} \le \theta \le 0\right]. \end{cases} \tag{5}$$

Given a specific set of circuit parameters provided in Table I, we can generate the '$P_{\text{Core}}^{\text{Meas}}$ vs. θ' curve by applying (5), as illustrated in Fig. 3. Ignoring higher-order terms, the sensitivity of the measured core loss to the timing skew is proportional to $V_L(V_H - V_L)/L$. When the current waveform leads the

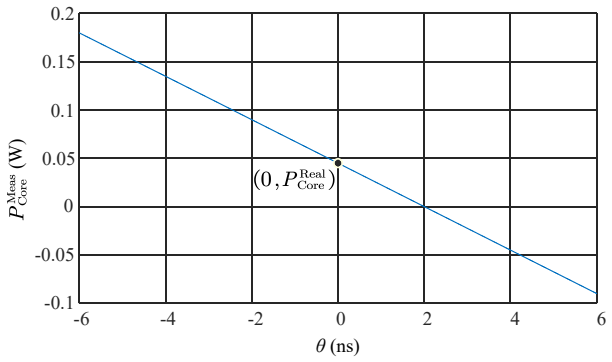

Fig. 3. Calculation result: $P_{\text{Core}}^{\text{Meas}}$ vs. θ

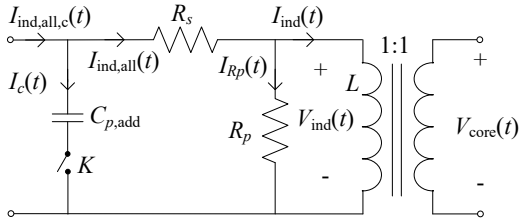

Fig. 4. Equivalent circuit model with $C_{p,\text{add}}$

voltage waveform (i.e., $\theta < 0$), the measured core loss will exceed the real core loss; on the contrary, if the current waveform lags the voltage waveform (i.e., $\theta > 0$), the measured core loss will be less than the real core loss, which often leads to an impossible "negative" core loss in conventional loss measurements. The real core loss can be read from the loss curve once the absolute zero-skew position is determined.

III. The Proposed Method

With the aid of an additional added capacitor, the direct *in-situ* inductor loss measurement is realized through the improved dual-curve derivative (iDCD) method from our previous work [25]. In this section, in conjunction with the two-winding method, we will explore the extension of the iDCD method to enable the direct core loss measurement, eliminating the measurement error introduced by the unknown timing skew. In this section, we will assess the feasibility of the proposed method by conducting an analysis employing our developed mathematical model and further validating it through simulation.

A. Theoretical analysis

To obtain the core loss from the direct measurement, the timing skew between measurement channels should be determined first. Here, a small additional capacitor, $C_{p,\text{add}}$, at a pF level is added across the inductor by a general switch K as shown in Fig. 4. When K is closed, current through the capacitor, I_c, will be introduced into the measured inductor current, $I_{\text{ind,all},c}$:

$$\begin{cases} I_{\text{ind,all},c}(t) = I_{\text{ind,all}}(t) + I_c(t) \\ V_{\text{core}}(t) = V_{\text{ind}}(t) \end{cases}, \tag{6}$$

where

$$I_c(t) = C_{p,\text{add}} \frac{d(V_{\text{ind}}(t) + (I_{\text{ind}}(t) + V_{\text{ind}}(t)/R_p) \cdot R_s)}{dt}. \tag{7}$$

The sensitivity of the measured core loss with respect to the timing skew without $C_{p,\text{add}}$, $\partial P_{\text{Core}}^{\text{Meas},1}(\theta)/\partial\theta$, can be calculated as

$$\frac{\partial P_{\text{Core}}^{\text{Meas},1}(\theta)}{\partial\theta} = \frac{\partial}{\partial\theta}\left[\frac{1}{T}\int_{t_0}^{t_0+T} V_{\text{ind}}(t)\, I_{\text{ind,all}}(t+\theta)\, \mathrm{d}t\right]. \tag{8}$$

Similarly, the sensitivity of the measured core loss with $C_{p,\text{add}}$, $\partial P_{\text{Core}}^{\text{Meas},2}(\theta)/\partial\theta$, can be expressed as

$$\frac{\partial P_{\text{Core}}^{\text{Meas},2}(\theta)}{\partial\theta} = \frac{\partial}{\partial\theta}\left[\frac{1}{T}\int_{t_0}^{t_0+T} V_{\text{ind}}(t)\, I_{\text{ind,all},c}(t+\theta)\, \mathrm{d}t\right]. \tag{9}$$

The superscripts "1" and "2" denote the cases without and with $C_{p,\text{add}}$, respectively. According to (8) and (9), the difference between two loss measurement sensitivities, $\Delta\partial P_{\text{Core}}^{\text{Meas}}(\theta)/\partial\theta$, can be obtained as

$$\begin{aligned} \Delta\frac{\partial P_{\text{Core}}^{\text{Meas}}(\theta)}{\partial\theta} &= \frac{\partial P_{\text{Core}}^{\text{Meas},1}(\theta)}{\partial\theta} - \frac{\partial P_{\text{Core}}^{\text{Meas},2}(\theta)}{\partial\theta} \\ &= -\frac{\partial P_{\text{Core,}c}^{\text{Meas}}(\theta)}{\partial\theta}, \end{aligned} \tag{10}$$

where $\partial P_{\text{Core,}c}^{\text{Meas}}(\theta)/\partial\theta$ represents the derivative items related to $C_{p,\text{add}}$ and can be expressed as

$$\frac{\partial P_{\text{Core,}c}^{\text{Meas}}(\theta)}{\partial\theta} = \frac{\partial}{\partial\theta}\left[\frac{1}{T}\int_{t_0}^{t_0+T} V_{\text{ind}}(t)\, I_c(t+\theta)\, \mathrm{d}t\right]. \tag{11}$$

Substituting (7) into (11) and combining the expressions of $V_{\text{ind}}(t)$, $I_{\text{ind}}(t+\theta)$ and $V_{\text{ind}}(t+\theta)$, $\partial P_{\text{Core,}c}^{\text{Meas}}(\theta)/\partial\theta$ can be calculated as

$$\frac{\partial P_{\text{Core,}c}^{\text{Meas}}(\theta)}{\partial\theta} = \begin{cases} * \ \frac{C_{p,\text{add}}R_sS^2f}{L}\theta^2 - 2C_{p,\text{add}}fS^2\left(1+\frac{R_s}{R_p}+\frac{R_sV_H}{LS}\right)\theta \\ \quad + 2C_{p,\text{add}}fSV_H\left(1+\frac{R_s}{R_p}\right) \\ \dagger - \frac{C_{p,\text{add}}R_sS^2f}{L}\theta^2 + 2C_{p,\text{add}}fS^2\left(1+\frac{R_s}{R_p}-\frac{R_sV_H}{LS}\right)\theta \\ \quad + 2C_{p,\text{add}}fSV_H\left(1+\frac{R_s}{R_p}\right) \\ *\left[\text{For } 0 \le \theta \le \frac{V_H}{S}\right], \dagger\left[\text{For } -\frac{V_H}{S} \le \theta \le 0\right]. \end{cases} \tag{12}$$

In a practical case, the magnitude of $\frac{R_sV_H}{LS}$ is usually much smaller than 1. Under such an assumption, $\partial^2 P_{\text{Core,}c}^{\text{Meas}}(\theta)/\partial\theta^2$ is negative for $0 \le \theta \le V_H/S$ and positive for $-V_H/S \le \theta \le 0$ because:

$$\frac{\partial^2 P_{\text{Core,}c}^{\text{Meas}}(\theta)}{\partial\theta^2} = \begin{cases} * \ 2C_{p,\text{add}}fS^2\left(\frac{R_s}{L}\theta - \frac{R_sV_H}{LS} - 1 - \frac{R_s}{R_p}\right) < 0 \\ \dagger - 2C_{p,\text{add}}fS^2\left(\frac{R_s}{L}\theta + \frac{R_sV_H}{LS} - 1 - \frac{R_s}{R_p}\right) > 0 \\ *\left[\text{For } 0 \le \theta \le \frac{V_H}{S}\right], \dagger\left[\text{For } -\frac{V_H}{S} \le \theta \le 0\right]. \end{cases} \tag{13}$$

Thus, in a real measurement, the nadir point of "$\Delta\partial P_{\text{Core}}^{\text{Meas}}(\theta)/\partial\theta$ vs. θ" curve can pinpoint the location where the absolute timing skew is zero. Based on the circuit parame-

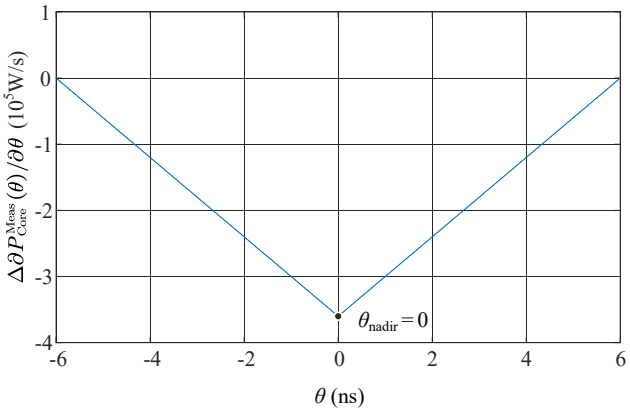

Fig. 5. $\Delta\partial P_{\text{Core}}^{\text{Meas}}(\theta)/\partial\theta$ vs. θ in calculation

ters exemplified in Section II, the curve of "$\Delta\partial P_{\text{Core}}^{\text{Meas}}(\theta)/\partial\theta$ vs. θ" is illustrated in Fig. 5. The nadir point of the plot reports the absolute zero-skew point. Thus, the proposed method enables direct core loss measurement through the following steps:

(1) Set up the two-winding method in the circuit to measure the inductor current and core voltage waveforms.

(2) Obtain $P_{\text{Core}}^{\text{Meas},1}$ vs. θ without the additional $C_{p,\text{add}}$.

(3) Obtain $P_{\text{Core}}^{\text{Meas},2}$ vs. θ with the additional $C_{p,\text{add}}$.

(4) Calculate $\Delta\partial P_{\text{Core}}^{\text{Meas}}(\theta)/\partial\theta$ vs. θ, where $\Delta\partial P_{\text{Core}}^{\text{Meas}} = P_{\text{Core}}^{\text{Meas},1} - P_{\text{Core}}^{\text{Meas},2}$.

(5) Plot '$\Delta\partial P_{\text{Core}}^{\text{Meas}}(\theta)/\partial\theta$ vs. θ' and find $\theta = \theta_0$ where the curve reaches its minimum. θ_0 represents the actual timing skew.

(6) Return to Step (2) and obtain the actual core loss by reading $P_{\text{Core}}^{\text{Meas},1}(\theta_0)$.

It is essential to highlight that the introduction of an additional capacitor in step (3) may lead to extra current ripples, which can marginally influence the magnetic loss. Nevertheless, this current distortion serves a specific purpose: precisely identifying the actual timing skew as a timing marker. The actual core loss is determined by referencing the initial core loss curve without incorporating this added capacitor. Consequently, any distortions in the measured current waveform resulting from the added capacitor do not affect the accuracy of the core loss determination. In addition, the parasitic capacitance of a real inductor can be modeled as a lumped capacitor across the inductor. While this introduces an additional current dip during transitions, it does not impact the loss difference derivative items introduced by the added capacitance [25]. Thus, it does not affect the effectiveness of the proposed method.

B. Simulation Verification

To validate the theoretical analysis of the proposed method, a DC-DC step-down buck converter is built in a circuit simulator, as in Fig. 6. Spice models of GaN MOSFET GS66508B

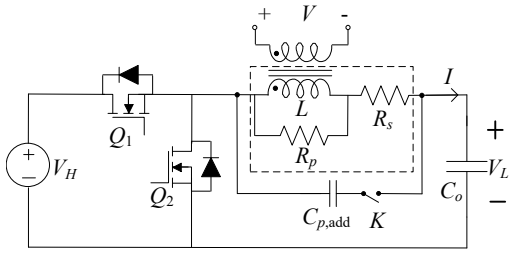

Fig. 6. Simulation circuit

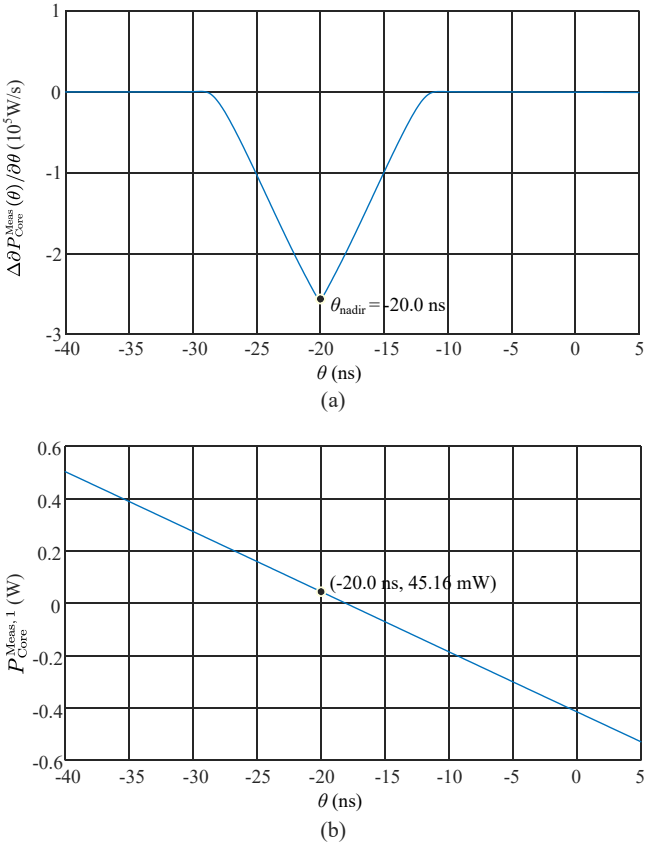

Fig. 7. Simulation verification of the proposed method. (a) '$\Delta\partial P_{\text{Core}}^{\text{Meas}}(\theta)/\partial\theta$ vs. θ' curve. (b) '$P_{\text{Core}}^{\text{Meas},1}$ vs. θ' curve.

are used for switching devices Q_1 and Q_2. The inductor is constructed based on the equivalent circuit model in Fig. 2. The two-winding method is applied to obtain the core voltage by utilizing an auxiliary winding with a unity turns ratio. A capacitor, $C_{p,\text{add}}$, is added across the inductor and controlled by a switch K. The main circuit parameters are given in Table I.

Simulation is performed following the steps listed in Section III-A. Next, the switch K is closed and the additional capacitor $C_{p,\text{add}}$ is added across the inductor. Other circuit parameters remain unchanged. The inductor current and core voltage waveforms are recorded again in the steady state. Two sets of inductor current and core voltage waveforms, one without and one with $C_{p,\text{add}}$, are collected for subsequent data processing.

Before processing the data, an arbitrary timing skew of 20 ns

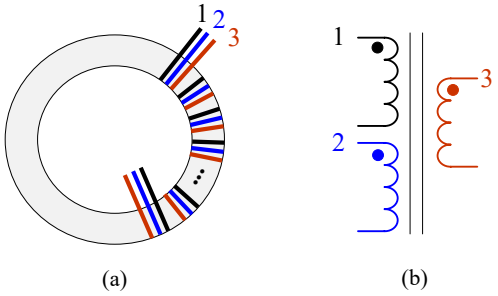

Fig. 8. An inductor for the Three-winding method. (a) Physical diagram. (b) Equivalent circuit.

is applied to delay the current waveforms for both simulation results, which serves as an unknown timing skew in reality. Then, two "P vs. θ" curves without and with $C_{p,\text{add}}$ are generated by sweeping an artificial timing skew θ on current waveforms in MATLAB. The derivatives of two measured core losses with respect to θ are calculated and the difference between them, $\Delta\partial P_{\text{Core}}^{\text{Meas}}(\theta)/\partial\theta$, is obtained as illustrated in Fig. 7 (a). The nadir point of the "$\Delta\partial P_{\text{Core}}^{\text{Meas}}(\theta)/\partial\theta$ vs. θ" curve successfully pinpoints the actual timing skew as $-20\,\text{ns}$. Based on this pinpointed timing skew of $-20\,\text{ns}$, the core loss can be read from the original, unmodified "$P_{\text{Core}}^{\text{Meas},1}$ vs. θ" curve. The resulting core loss is $45.16\,\text{mW}$ as shown in Fig. 7 (b) and is identical to the core loss directly reported by the simulator. The simulation result successfully proves the validity of the theoretical analysis.

IV. Experimental Verification

In this section, a novel cross-verification method is first designed to establish a core loss reference for experimental verification. The proposed core loss measurement method is then assessed in a dedicated experimental platform. The experimental results will be evaluated in comparison to the established core loss reference. Various circuit parameters and inductors will be systematically tested and analyzed.

A. The Three-winding Method

With our previously developed iDCD method [25], the total inductor loss can be accurately measured *in-situ* and in-operation. Given the measured total inductor loss, the core loss can be obtained if the winding loss is known. In an effort to experimentally identify the winding loss based on the deduction method, a special inductor with three windings is designed, as illustrated in Fig. 8. Three identical windings, denoted as winding 1, winding 2, and winding 3, are uniformly wound onto the target magnetic core.

Two measurements will be conducted to obtain the core loss reference of interest ($P_{\text{Core}}^{\text{ref}}$). In the initial measurement setup, the three-winding inductor is connected to the converter circuit as follows: winding 1 is left unconnected (floating), winding 2 serves as the inductor winding within the power loop, and winding 3 functions as the auxiliary winding responsible for core voltage extraction. The winding resistance of the inductor can be regarded as $R_{s,1}$. In the first measurement, the converter is operated under specified conditions, with the enforcement of ZVS operation for the MOSFETs to simplify the converter's loss mechanism. The inductor loss, $P_{\text{ind},1}$, can be measured based on the iDCD method. Furthermore, the input power ($P_{in,1}$) and the output power ($P_{o,1}$) of the converter can be directly measured to calculate the total converter loss, $P_{\text{loss},1}$.

$$P_{\text{loss},1} = P_{in,1} - P_{o,1}. \tag{14}$$

Considering the loss mechanism of the converter,

$$P_{\text{loss},1} = P_{\text{FET},1} + P_{\text{core},1} + P_{\text{winding},1} + P_{\text{other},1}, \tag{15}$$

where P_{FET}, P_{core}, P_{winding}, and P_{other} represent the FET loss, core loss, winding loss, and other losses, respectively. The subscript "1" denotes the first measurement.

In the second measurement, while keeping the same circuit parameters and configuration, we parallel winding 1 with winding 2 to form the inductor winding. The winding loss in the second measurement should be reduced to $R_{s,2}$. With a relatively simple winding structure as shown in Fig. 8 (a), it is straightforward that the inductance will remain consistent with the first measurement and $R_{s,2} = R_{s,1}/2$, as winding 1 and winding 2 are identical. The input power ($P_{in,2}$) and output power ($P_{o,2}$) of the converter are measured again to get the converter loss $P_{\text{loss},2}$.

$$P_{\text{loss},2} = P_{in,2} - P_{o,2}. \tag{16}$$

Similarly,

$$P_{\text{loss},2} = P_{\text{FET},2} + P_{\text{core},2} + P_{\text{winding},2} + P_{\text{other},2}. \tag{17}$$

The subscript "2" represents the second measurement. Assuming that the inductor current remains consistent in both measurements, the FET loss, core loss, and other losses will remain unchanged, while the winding loss should be halved:

$$P_{\text{winding},2} = 0.5 P_{\text{winding},1}. \tag{18}$$

This implies that the difference between the two total converter losses equals half of the winding loss observed in the first measurement. Consequently, we can estimate the specific winding loss of interest in the first measurement through the following relationship:

$$\begin{aligned} P_{\text{winding},1} &= 2\left(P_{\text{loss},1} - P_{\text{loss},2}\right) \\ &= 2\left[(P_{in,1} - P_{o,1}) - (P_{in,2} - P_{o,2})\right]. \end{aligned} \tag{19}$$

In reality, the inductor current in the second measurement will be slightly reduced due to a smaller winding resistance. Thus, the RMS values of the inductor currents, $I_{L,1}$ in the measurement and $I_{L,2}$ in the second measurement, should also be measured. Assuming a linear loss mechanism for the converter (i.e., "$P \propto I$"), the lower boundary of the winding loss estimation, denoted as $P_{\text{winding,L}}$, should be:

$$P_{\text{winding,L}} = 2\left[(P_{in,1} - P_{o,1}) - \frac{I_{L,1}}{I_{L,2}}(P_{in,2} - P_{o,2})\right]. \tag{20}$$

Considering that the converter's losses follows a quadratic relationship with current (i.e., '$P \propto I^2$'), the upper boundary of the winding loss estimation, denoted as $P_{\text{winding,H}}$, should

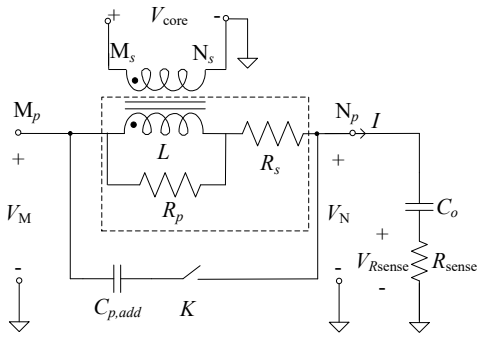

Fig. 9. Measurement diagram in experiment

be:

$$P_{\text{winding,H}} = 2\left[(P_{in,1} - P_{o,1}) - \frac{I_{L,1}^2}{I_{L,2}^2}(P_{in,2} - P_{o,2})\right]. \quad (21)$$

Again, this "assumed" behavior and unmodeled parasitics ultimately prevent a pinpointed value estimation and only provide an estimation band. However, it is much tighter in this controlled experiment than the conventional deduction method. Therefore, rather than a specific baseline, a relatively tighter estimation range can be obtained for the core loss reference by combining the winding loss boundaries (20) and (21) with the inductor loss determined in the first measurement:

$$[P_{\text{core,L}}, P_{\text{core,H}}] = [P_{\text{ind},1} - P_{\text{winding,H}}, P_{\text{ind},1} - P_{\text{winding,L}}], \quad (22)$$

where $P_{\text{core,L}}$ and $P_{\text{core,H}}$ represent the lower and upper boundaries of the core loss reference range. By employing the Three-winding method, a core loss reference range can be obtained in the experiment for cross verification. Note that the Three-winding method is only applicable in the lab under strictly controlled conditions. The accuracy of the reference range may be questionable when dealing with complex winding loss mechanisms, such as those with multi-layer winding structures. Note, however, that our goal is to demonstrate the accuracy of the proposed method using this cross-validation method.

In the following experiments, inductors equipped with three windings will be used. In addition to measuring the core loss of interest, the inductor loss will also be obtained based on the iDCD method to establish the core loss reference using the Three-winding method. Thus, the measurement diagram is shown in Fig. 9. Two passive voltage probes are positioned at both ends of the inductor to capture the inductor voltage (i.e., $V_{\text{M}} - V_{\text{N}}$). Another passive voltage probe is connected across the auxiliary winding to get the core voltage (i.e., V_{core}). To measure the inductor current, a sense resistor, R_{sense}, is utilized, and the voltage across the sense resistor, $V_{R\text{sense}}$, is recorded.

B. Experimental Verification

For experimental verification, a platform is set up as shown in Fig. 10. A buck converter is built with a half-bridge GaN E-HEMT daughter board (GS66508B-EVBDB1) and a mother board (GS665MB-EVB) from GaN Systems. The control signals are provided by the function generator. A custom measurement board is designed and built to realize low parasitic measurements and convenient connections. An inductor with three windings is constructed with a magnetic core (model number 58587A2) and the magnet wire of AWG 26 as shown in Fig. 11. Following Fig. 9, three passive voltage probes of 1 GHz bandwidth are utilized to measure inductor voltage and core voltage. Current probes allow easy and non-intrusive measurement of current waveforms. However, commercially available current probes typically have a limited bandwidth of less than 150 MHz. This bandwidth is insufficient to capture detailed current information during transitions, especially with wide bandgap devices like GaN, making these probes unsuitable for the proposed method since it relies on fine-resolution current measurement around the critical edges. Thus, a sense resistor approach, built with twenty 0402 resistors of 2 Ω, is employed to increase the bandwidth for current measurement. The voltage across the sense resistor is collected using a coaxial (MMCX) connector and fed into the oscilloscope through a coaxial cable for a GHz-level bandwidth. Ceramic capacitors rated as C0G (NP0) are employed for $C_{p,\text{add}}$ in the experiment to minimize capacitance variation and dielectric loss resulting from voltage and temperature changes. To facilitate connection control of $C_{p,\text{add}}$, a two-pin header and a jumper shunt are utilized as the switch K in the experiment. The equipment used is: CPX400S (DC power supply); AFG31000 (function generator); MSO64 (oscilloscope); TPP1000 (passive voltage

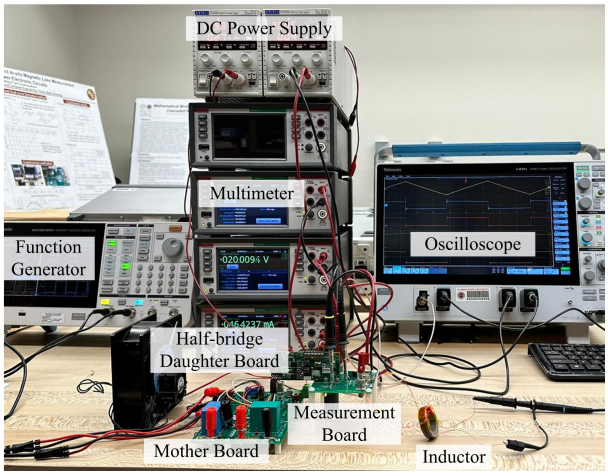

Fig. 10. Experimental platform

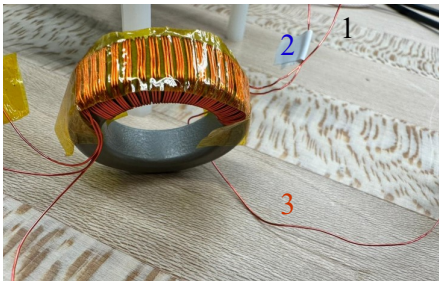

Fig. 11. An inductor for the Three-winding method

TABLE II
MAIN CIRCUIT PARAMETERS IN EXPERIMENT

V_H	V_L	f	L	Turns ratio	$C_{p,\text{add}}$	R_{sense}
30 V	15 V	100 kHz	9.2 µH	18:18	12 pF	97.9 mΩ

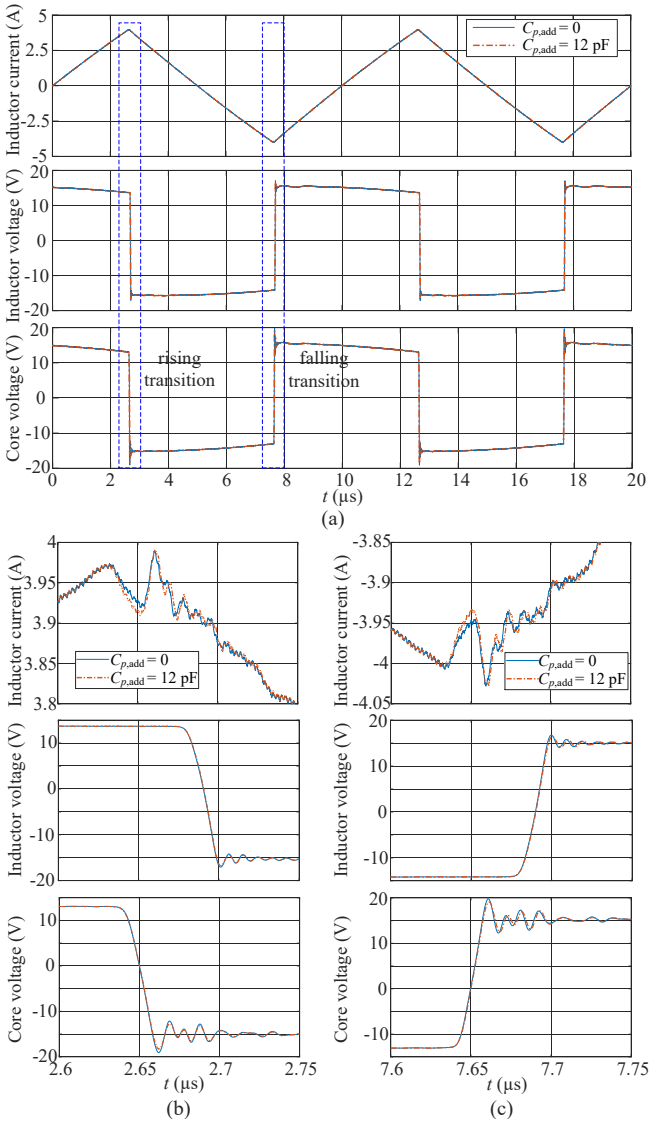

Fig. 12. Experimental waveforms in the time domain. (a) Waveforms in two switching cycles. (b) Waveforms during the rising transition. (c) Waveforms during the falling transition.

probe); and DMM6500 (multimeter). The oscilloscope's sample rate is 12.5 Gs/s. The experimental parameters are shown in Table II.

To simplify the loss mechanism, the output of the converter is open and the ZVS operation of the switches is realized in the experiment. For normal operation, winding 2 is connected to the converter and the winding 3 is connected to a voltage probe for core voltage measurement. Winding 1 is left floating. After the DC-DC buck converter reaches the steady state, the time-domain waveforms without and with the presence of $C_{p,\text{add}}$ are recorded in Fig. 12 (a), including the inductor current, inductor voltage, and core voltage. To offer a more detailed view of the rising and falling transitions, the zoomed-in representations are provided in Fig. 12 (b) and Fig. 12 (c), respectively. Both the inductor voltage and core voltage remain the same during the transition while the current waveform contains a deeper dip when $C_{p,\text{add}}$ is introduced. Note that the original current waveform already contains a certain current dip during the transition, primarily attributable to its parasitic capacitance. According to Fig. 12, it is evident that the measured current exhibits distinct timing skews relative to the inductor voltage and core voltage. The observed difference in two timing skews is approximately 40 ns. In addition to the waveforms, the input power ($P_{in,1}$) and the root mean square (RMS) values of the inductor current ($I_{L,1}$) are measured, yielding values of 2.481 W and 2.321 A, respectively, in the absence of $C_{p,\text{add}}$. The output power ($P_{o,1}$) is zero as the load is open.

To obtain the core loss reference, the Three-winding method is applied with winding 1 connected to the converter in parallel with winding 2 and the extra capacitor removed from the circuit. All the other circuit parameters remain the same. After the converter operates in steady state, the input power ($P_{in,2}$) and the RMS values of the inductor current ($I_{L,2}$) are measured again as 2.226 W and 2.343 A, respectively. According to (20) and (21), the winding loss reference range can be calculated as [552.737 mW, 595.015 mW]. Next, the iDCD method is applied to figure out the inductor loss, where the timing skew between the inductor current and inductor voltage is 43.34 ns and the real inductor loss is 1.248 W. According to (22), the core loss reference range can then be obtained as [652.265 mW, 694.543 mW].

Next, the inductor current and core voltage waveforms are processed in MATLAB following the steps of the proposed method. The curve of "$\Delta\partial P_{\text{Core}}^{\text{Meas}}(\theta)/\partial\theta$" is illustrated in Fig. 13 (a). The nadir point reports the actual timing skew between the inductor current and core voltage is 3.6 ns. The core loss curve without the extra capacitor $C_{p,\text{add}}$ is illustrated in Fig. 13 (b), where the real core loss, 672.2 mW, is then read from. To evaluate the repeatability of the proposed method in experiment, the measurement is repeated five times, yielding five sets of inductor current and core voltage waveforms. Fig. 14 displays the corresponding 25 results of the actual timing skew and real core loss. Statistical analysis of this dataset yielded the following findings: The mean timing skew is $\mu = 3.6224$ ns with a standard deviation of $\sigma = 0.0734$ ns. The mean core loss is $\mu = 671.652$ mW with a standard deviation of $\sigma = 1.6947$ mW. Incorporating the coupling coefficient (k) between winding 2 and winding 3, which is measured at 0.9983, the mean core loss is converted to be $\mu = 679.603$ mW with a standard deviation of $\sigma = 1.7148$ mW according to the equation below:

$$P_{\text{final}} = P_{\text{initial}}/k, \tag{23}$$

where P_{initial} and P_{final} are loss values before and after incorporating the coupling coefficient, respectively. The experimental measurements of the core loss are highly concentrated in a narrow range, with all results falling within the core loss reference range established by the Three-winding method. Without the proposed method, the direct measured core loss, $P_{\text{Core}}^{\text{Direct}}$, is 758.0 mW, which is out of the core loss reference

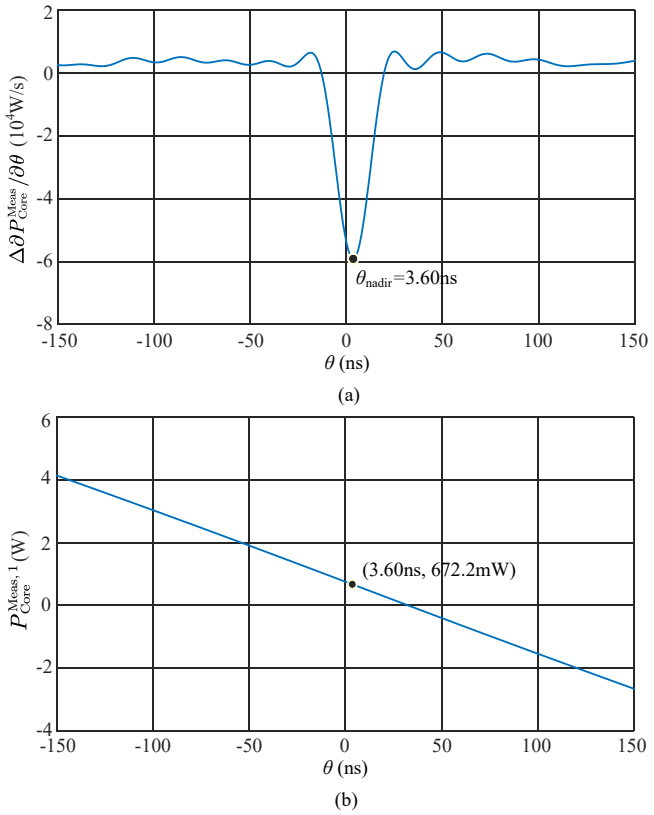

Fig. 13. Experimental validation of the proposed method. (a) '$\Delta\partial P_{\text{Core}}^{\text{Meas}}(\theta)/\partial\theta$ vs. θ' curve. (b) '$P_{\text{Core}}^{\text{Meas},1}$ vs. θ' curve.

range. Taking the proposed method as the reference, the error in the direct measured core loss is 11.54%. The experimental results effectively confirm the validity of the theoretical analysis of the proposed core loss measurement method, confirming its accuracy and practical applicability.

C. Further Experimental Verification with Various Parameters

To comprehensively evaluate the proposed core loss measurement method, the experiment is repeated with different circuit parameters. With the parameters in Table II as default values, different experiment sets are conducted at different voltages, duty ratios, loads, and frequencies. For each experimental set, the Three-winding method is employed to establish the core loss reference range. Utilizing five sets of recorded waveforms, 25 experimental samples are calculated to derive the mean and standard deviation values for both the actual timing skew and the real core loss. The experiment is carried out at the input voltage of 20 V, 30 V, and 40 V. The results of the actual timing skew and real core loss are shown in Table III. Similarly, the converter is tested at the duty ratio of 0.2, 0.5, and 0.7. The actual timing skew and real core loss are given in Table IV. As the output voltage is 15 V, the load current is regulated to 0.75 A and 1.5 A by modifying the load resistance to 20 Ω and 10 Ω, respectively. The results of different loads are provided in Table V. To evaluate the experiment under different switching frequencies while utilizing the same inductor, tests are conducted at 250 kHz, 500 kHz, and 1 MHz. To meet

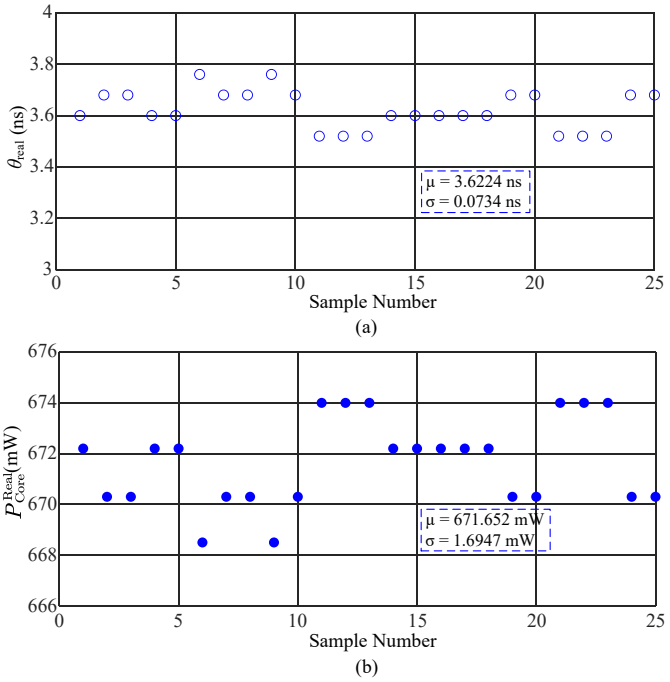

Fig. 14. 25 experimental results of the proposed method. (a) Actual timing skew. (b) Actual core loss.

TABLE III
EXPERIMENTAL VALIDATION WITH DIFFERENT INPUT VOLTAGES

V_H(V)	θ_{real}(ns)		$P_{\text{Core}}^{\text{Real}}$(mW)		$P_{\text{Core}}^{\text{ref}}$(mW)	$P_{\text{Core}}^{\text{Direct}}$ (mW)	$\frac{P_{\text{Core}}^{\text{Direct}}-P_{\text{Core}}^{\text{Real}}}{P_{\text{Core}}^{\text{Real}}}$
	Mean (μ)	SD (1-σ)	Mean (μ)	SD (1-σ)			
20	3.626	0.077	**272.52**	**0.817**	[162.196, 280.843]	305.4	12.07%
30	3.622	0.073	**679.603**	**1.715**	[652.265, 694.543]	758.0	11.54%
40	3.619	0.052	**1298.472**	**1.973**	[1239.84, 1360.65]	1437.0	10.67%

TABLE IV
EXPERIMENTAL VALIDATION WITH DIFFERENT DUTY RATIOS

D	θ_{real}(ns)		$P_{\text{Core}}^{\text{Real}}$(mW)		$P_{\text{Core}}^{\text{ref}}$(mW)	$P_{\text{Core}}^{\text{Direct}}$ (mW)	$\frac{P_{\text{Core}}^{\text{Direct}}-P_{\text{Core}}^{\text{Real}}}{P_{\text{Core}}^{\text{Real}}}$
	Mean (μ)	SD (1-σ)	Mean (μ)	SD (1-σ)			
0.2	3.728	0.045	**295.898**	**0.640**	[285.906, 309.923]	346.4	17.07%
0.5	3.622	0.073	**679.603**	**1.715**	[652.265, 694.543]	758.0	11.54%
0.7	3.552	0.045	**511.853**	**0.905**	[481.157, 528.136]	577.0	12.73%

TABLE V
EXPERIMENTAL VALIDATION WITH DIFFERENT LOADS

Load(A)	θ_{real}(ns)		$P_{\text{Core}}^{\text{Real}}$(mW)		$P_{\text{Core}}^{\text{ref}}$(mW)	$P_{\text{Core}}^{\text{Direct}}$ (mW)	$\frac{P_{\text{Core}}^{\text{Direct}}-P_{\text{Core}}^{\text{Real}}}{P_{\text{Core}}^{\text{Real}}}$
	Mean (μ)	SD (1-σ)	Mean (μ)	SD (1-σ)			
0	3.622	0.073	**679.603**	**1.715**	[652.265, 694.543]	758.0	11.54%
0.75	3.619	0.065	**765.585**	**1.540**	[692.320, 776.478]	853.5	10.18%
1.5	3.686	0.071	**842.380**	**1.683**	[797.958, 866.953]	918.2	9.00%

the ZVS requirement, the inductance is reduced to 3.0 μH, while other parameters remain the same as the default values. The experimental results of different frequencies are shown in Table VI. Though the timing skew remains similar across different switching frequencies, the impact of the error increases significantly with higher frequencies.

Subsequently, experiments are conducted with various magnetic components. Different inductances of 6.89 μH, 9.20 μH, and 15.49 μH are achieved by modifying the number of turns in the windings while with the same magnetic core. Next, the cross-sectional area of the winding wire is adjusted by replacing

TABLE VI
EXPERIMENTAL VALIDATION WITH DIFFERENT FREQUENCIES

f(kHz)	θ_{real}(ns)		$P_{\text{Core}}^{\text{Real}}$(mW)		$P_{\text{Core}}^{\text{ref}}$(mW)	$P_{\text{Core}}^{\text{Direct}}$ (mW)	$\frac{P_{\text{Core}}^{\text{Direct}}-P_{\text{Core}}^{\text{Real}}}{P_{\text{Core}}^{\text{Real}}}$
	Mean (μ)	SD (1-σ)	Mean (μ)	SD (1-σ)			
250	3.670	0.057	**1002.811**	**3.876**	[974.883, 1091.804]	1205.0	20.16%
500	3.606	0.055	**629.762**	**3.598**	[606.344, 668.998]	837.9	33.05%
1000	3.386	0.044	**392.173**	**2.809**	[358.382, 407.137]	592.7	51.13%

TABLE VII
EXPERIMENTAL VALIDATION WITH DIFFERENT INDUCTANCES

L(μH)	θ_{real}(ns)		$P_{\text{Core}}^{\text{Real}}$(mW)		$P_{\text{Core}}^{\text{ref}}$(mW)	$P_{\text{Core}}^{\text{Direct}}$ (mW)	$\frac{P_{\text{Core}}^{\text{Direct}}-P_{\text{Core}}^{\text{Real}}}{P_{\text{Core}}^{\text{Real}}}$
	Mean (μ)	SD (1-σ)	Mean (μ)	SD (1-σ)			
6.89	3.472	0.078	**1087.29**	**2.477**	[993.250, 1112.021]	1165.0	7.15%
9.20	3.622	0.073	**679.603**	**1.715**	[652.265, 694.543]	758.0	11.54%
15.49	3.725	0.051	**452.335**	**0.717**	[433.101, 457.221]	492.6	8.90%

TABLE VIII
EXPERIMENTAL VALIDATION WITH DIFFERENT WINDINGS

Winding	θ_{real}(ns)		$P_{\text{Core}}^{\text{Real}}$(mW)		$P_{\text{Core}}^{\text{ref}}$(mW)	$P_{\text{Core}}^{\text{Direct}}$ (mW)	$\frac{P_{\text{Core}}^{\text{Direct}}-P_{\text{Core}}^{\text{Real}}}{P_{\text{Core}}^{\text{Real}}}$
	Mean (μ)	SD (1-σ)	Mean (μ)	SD (1-σ)			
A	3.674	0.071	**727.718**	**1.680**	[626.090, 748.930]	800.0	9.93%
B	3.622	0.073	**679.603**	**1.715**	[652.265, 694.543]	758.0	11.54%
C	3.555	0.064	**1297.096**	**2.260**	[1203.321, 1334.506]	1388.0	7.01%

TABLE IX
EXPERIMENTAL VALIDATION WITH DIFFERENT CORES

Core	θ_{real}(ns)		$P_{\text{Core}}^{\text{Real}}$(mW)		$P_{\text{Core}}^{\text{ref}}$(mW)	$P_{\text{Core}}^{\text{Direct}}$ (mW)	$\frac{P_{\text{Core}}^{\text{Direct}}-P_{\text{Core}}^{\text{Real}}}{P_{\text{Core}}^{\text{Real}}}$
	Mean (μ)	SD (1-σ)	Mean (μ)	SD (1-σ)			
A	3.613	0.063	**285.384**	**1.346**	[264.196, 287.497]	357.3	25.20%
B	3.622	0.073	**679.603**	**1.715**	[652.265, 694.543]	758.0	11.54%
C	3.677	0.073	**902.623**	**1.590**	[877.156, 908.431]	962.5	6.63%

it with different magnet wires (i.e., AWG 30, AWG 26, and AWG 22). Note that the inductances of the three inductors vary as a result of differences in turn-to-turn spacing. Finally, three different cores (i.e., 58440A2, 58587A2, and 58154A2) are tested where the number of turns in the windings are adjusted to keep the inductance similar. Other circuit parameters remain the same as the default values. The actual timing skew and real core loss for the three different inductors are provided in Table VII, Table VIII, and Table IX, respectively.

The data displayed in all the tables clearly demonstrate that there are minimal fluctuations in actual timing skew and real core loss. Furthermore, it is noteworthy that all the obtained core loss values fall within the established core loss reference range from the Three-winding method. The experimental results prove the effectiveness of the proposed method over a wide range of circuit and design parameters.

D. Remarks on the Proposed Method

It should be noted that the ZVS operation is not necessary for the proposed core loss measurement method. It is adopted in this article to simplify the loss mechanism of the converter and obtain a more accurate and reliable core loss reference range. In addition, the Three-winding method is utilized in our experimental setup for the sole purpose of acquiring a core loss reference, allowing for cross-verification. In practical applications, there are no limitations regarding the type of winding or magnetic core that can be employed. The proposed method can be effectively applied where a magnetic component operates under rectangular voltage excitation, provided that precise measurements of inductor current and core voltage can be reliably obtained. In real-world measurements, the presence of inevitable parasitic elements introduces high-frequency ripples into the recorded current and voltage waveforms. These ripples, if left unaddressed, have the potential to distort the derivative curve used to determine the actual timing skew. To mitigate this effect, mathematical tools can be employed to eliminate high-frequency components. For example, we have eliminated 16th harmonic and beyond via an FFT filter for the data processing in this paper. In addition, since the proposed method is built on the traditional two-winding method, it is necessary to maintain a high coupling coefficient and account for it in the final core loss calculation as (23) suggests. A high coupling coefficient close to the unity is preferred as it reduces the introduced parasitics and mitigates ripples in the measurement. The proposed magnetic core loss measurement method is currently suitable only for inductors under rectangular voltage and triangular current excitation. It is not yet applicable for general *in-situ* core loss measurement of transformers with arbitrary waveforms in input and output. However, the method can be used for transformers with rectangular voltage excitation if the core loss is measured separately using a similar two-winding setup. For other topologies with non-rectangular voltage excitations or different transformer configurations, the loss models can vary significantly. In such cases, the analysis steps described in this article can be followed to derive new error models. Exploring new variables in these topologies could potentially lead to the development of a different in-situ measurement method.

V. CONCLUSION

The effect of the timing skew between the voltage and current measurement channels on direct magnetic core loss measurement under rectangular voltage excitation is analyzed. A mathematical model is established to represent the measured core loss as a function of the timing skew, covering the entire transition. The proposed method utilizes a pF-level additional capacitor to introduce a geometric characteristic to the mathematical model. This facilitates the accurate determination of the actual timing skew and the real magnetic core loss. This article also introduces the Three-winding method to provide a core loss reference range for cross verification in the laboratory. The effectiveness of the proposed core loss measurement method is verified through simulations and experiments under various circuit and design parameters, validating its ability to provide reliable and precise results. This approach enhances the understanding and analysis of the timing skew and its impact on the measured magnetic core losses. Building on previous work that measured total inductor loss, the proposed method now enables real-time measurement and distinction of core and winding losses. For the first time, a single, straightforward measurement setup can accurately capture both core and winding losses *in-situ*. This breakthrough has significant potential to contribute to the design and optimization of magnetic components in various applications.

VI. ACKNOWLEDGMENT

We acknowledge the generous support of Dr. Douglas Baney and Keysight Technologies.

REFERENCES

[1] Q. Huang, Y. Yang, Z. Ma, Y. Lai, and S. Wang, "Transformer structure of bifilar primary winding with advanced common mode noise attenuation performance for isolated dc-dc converters," in *2023 IEEE Applied Power Electronics Conference and Exposition (APEC)*, 2023, pp. 441–448.

[2] Y. Wang and T. Zhao, "A hybrid voltage regulation transformer based on interline power converters," in *2022 IEEE Applied Power Electronics Conference and Exposition (APEC)*, 2022, pp. 404–409.

[3] S. P. Martin, X. Dong, and H. Li, "Model development and predictive control of a low-inertia dc solid-state transformer (sst)," *IEEE Journal of Emerging and Selected Topics in Power Electronics*, vol. 10, no. 6, pp. 6482–6494, 2022.

[4] Z. Zhang, C. Liu, M. Wang, Y. Si, Y. Liu, and Q. Lei, "High-efficiency high-power-density cllc resonant converter with low-stray-capacitance and well-heat-dissipated planar transformer for ev on-board charger," *IEEE Transactions on Power Electronics*, vol. 35, no. 10, pp. 10 831–10 851, 2020.

[5] L. Yi and J. Moon, "Novel methods for in-situ direct magnetic loss measurement in a dc-dc converter," in *2020 IEEE Applied Power Electronics Conference and Exposition (APEC)*, 2020, pp. 61–69.

[6] ——, "Direct in-situ measurement of magnetic loss in power electronic circuits," *IEEE Transactions on Power Electronics*, vol. 36, no. 3, pp. 3247–3257, 2021.

[7] D. Conroy, G. Pierce, and P. Troyk, "Measurement techniques for the design of high-frequency smps transformers," in *APEC '88 Third Annual IEEE Applied Power Electronics Conference and Exposition*, 1988, pp. 341–351.

[8] R. Linkous, A. Kelley, and K. Armstrong, "An improved calorimeter for measuring the core loss of magnetic materials," in *APEC 2000. Fifteenth Annual IEEE Applied Power Electronics Conference and Exposition (Cat. No.00CH37058)*, vol. 2, 2000, pp. 633–639 vol.2.

[9] S. Bolte, N. Fröhleke, and J. Böcker, "Dc-dc converter design for power distribution systems in electric vehicles using calorimetric loss measurements," in *2016 18th European Conference on Power Electronics and Applications (EPE'16 ECCE Europe)*, 2016, pp. 1–7.

[10] J.-M. Yook, J.-H. Ko, M.-L. Ha, and Y.-S. Kwon, "High-quality solenoid inductor using dielectric film for multichip modules," *IEEE Transactions on Microwave Theory and Techniques*, vol. 53, no. 6, pp. 2230–2234, 2005.

[11] L. Yang, S. M. Gubanski, Y. V. Serdyuk, and J. Schiessling, "Dielectric properties of transformer oils for hvdc applications," *IEEE Transactions on Dielectrics and Electrical Insulation*, vol. 19, no. 6, pp. 1926–1933, 2012.

[12] J. Brittain, "A steinmetz contribution to the ac power revolution," *Proceedings of the IEEE*, vol. 72, no. 2, pp. 196–197, 1984.

[13] J. Muhlethaler, J. Biela, J. W. Kolar, and A. Ecklebe, "Improved core-loss calculation for magnetic components employed in power electronic systems," *IEEE Transactions on Power Electronics*, vol. 27, no. 2, pp. 964–973, 2012.

[14] M. Albach, T. Durbaum, and A. Brockmeyer, "Calculating core losses in transformers for arbitrary magnetizing currents a comparison of different approaches," in *PESC Record. 27th Annual IEEE Power Electronics Specialists Conference*, vol. 2, 1996, pp. 1463–1468 vol.2.

[15] J. Reinert, A. Brockmeyer, and R. De Doncker, "Calculation of losses in ferro- and ferrimagnetic materials based on the modified steinmetz equation," *IEEE Transactions on Industry Applications*, vol. 37, no. 4, pp. 1055–1061, 2001.

[16] J. Li, T. Abdallah, and C. Sullivan, "Improved calculation of core loss with nonsinusoidal waveforms," in *Conference Record of the 2001 IEEE Industry Applications Conference. 36th IAS Annual Meeting (Cat. No.01CH37248)*, vol. 4, 2001, pp. 2203–2210 vol.4.

[17] K. Venkatachalam, C. Sullivan, T. Abdallah, and H. Tacca, "Accurate prediction of ferrite core loss with nonsinusoidal waveforms using only steinmetz parameters," in *2002 IEEE Workshop on Computers in Power Electronics, 2002. Proceedings.*, 2002, pp. 36–41.

[18] V. Thottuvelil, T. Wilson, and H. Owen, "High-frequency measurement techniques for magnetic cores," *IEEE Transactions on Power Electronics*, vol. 5, no. 1, pp. 41–53, 1990.

[19] M. Mu, Q. Li, D. J. Gilham, F. C. Lee, and K. D. T. Ngo, "New core loss measurement method for high-frequency magnetic materials," *IEEE Transactions on Power Electronics*, vol. 29, no. 8, pp. 4374–4381, 2014.

[20] M. Mu, F. C. Lee, Q. Li, D. Gilham, and K. D. T. Ngo, "A high frequency core loss measurement method for arbitrary excitations," in *2011 Twenty-Sixth Annual IEEE Applied Power Electronics Conference and Exposition (APEC)*, 2011, pp. 157–162.

[21] D. Hou, M. Mu, F. C. Lee, and Q. Li, "New high-frequency core loss measurement method with partial cancellation concept," *IEEE Transactions on Power Electronics*, vol. 32, no. 4, pp. 2987–2994, 2017.

[22] Z. Ma, J. Yao, Y. Li, and S. Wang, "Comparative analysis of magnetic core loss measurement methods with arbitrary excitations," in *2019 IEEE Energy Conversion Congress and Exposition (ECCE)*, 2019, pp. 4125–4130.

[23] J. Moon, "In-situ direct magnetic loss measurement in a dc-dc converter," in *2019 IEEE Energy Conversion Congress and Exposition (ECCE)*, 2019, pp. 1261–1268.

[24] L. Yi and J. Moon, "In situ direct magnetic loss measurement with improved accuracy for lossier magnetics," *IEEE Transactions on Instrumentation and Measurement*, vol. 71, pp. 1–14, 2022.

[25] L. Yi, M. McTigue, D. Gines, B. Doerr, and J. Moon, "Minimally invasive direct in-situ magnetic loss measurement in power electronic circuits," *IEEE Transactions on Power Electronics*, pp. 1–11, 2023.